Available online at www.sciencedirect.com
SCIENCE DIRECT®
Optics Communications 232 (2004) 123–128
OPTICS COMMUNICATIONS
www.elsevier.com/locate/optcom

Dynamic focus control in high-speed optical coherence tomography based on a microelectromechanical mirror

Bing Qi [a,*], A. Phillip Himmer [b], L. Maggie Gordon [c], X.D. Victor Yang [c], L. David Dickensheets [b], I. Alex Vitkin [a,c,d]

[a] Ontario Cancer Institute/University Health Network, Toronto, ON, Canada M5G 2M9
[b] Department of Electrical and Computer Engineering, Montana State University, Bozeman, MT 59717, USA
[c] Department of Medical Biophysics, University of Toronto, Toronto, ON, Canada M5G 2M9
[d] Department of Radiation Oncology, University of Toronto, ON, Canada M5G 2M9

Received 15 December 2003; received in revised form 5 January 2004; accepted 9 January 2004

Abstract

In high-resolution optical coherence tomography (OCT), a high numerical aperture sample lens is required to achieve high lateral resolution. This situation leads to a limited depth of focus, which can yield sub-optimal lateral resolution outside the focal zone for deep-imaging OCT systems. To maintain high transverse resolution over the entire depth scan, we designed a high-speed dynamic focus control system based on a microelectromechanical mirror. The silicon nitride deformable mirror shifted the focus of the sample beam of the OCT interferometer in synchrony with the coherence-gate scan in the reference arm. As a result, the coherence gate remained at the beam focus during the whole imaging process. The prototype focus control setup was integrated into a high-speed (8 kHz depth scan frequency) OCT system. Improvement to the image quality was demonstrated with a standard resolution target.

PACS: 07.60–j; 07.10.Cm

Keywords: Optical coherence tomography; Microelectromechanical systems; Dynamic focus control

1. Introduction

Optical coherence tomography (OCT) is a fairly new optical imaging technique that permits three-dimensional high-resolution imaging in highly scattering media [1]. It is an analogous to ultrasound imaging except light waves instead of acoustic waves are employed in OCT systems.

* Corresponding author. Department of Physics, University of Toronto, 60 St. George Street, Toronto, Canada M5S1A7. Tel.: +4169785226; fax: +4169782537.
E-mail address: bqi@physics.utoronto.ca (B. Qi).

0030-4018/$ - see front matter © 2004 Published by Elsevier B.V.
doi:10.1016/j.optcom.2004.01.015

Backscattered photons from scattering sites inside a sample are localized in depth by low-coherence interferometry. An axial depth scan (A-scan in ultrasound imaging nomenclature) is achieved by scanning the reference delay line while recording the output from the interferometer. With sequential transverse scans, two- or three-dimensional images can be obtained.

From a clinical perspective, high resolution and high frame rates are two crucial parameters for any medical imaging system. In a standard OCT system, the axial (depth) resolution is determined primarily by the coherence length of light source, whereas the lateral (transverse) resolution depends on the numerical aperture of the probe beam [2]. In principle, the axial resolution could be improved by using a light source with a larger spectral bandwidth [3]. The use of a high numerical aperture lens in the probe improves lateral resolution, but also decreases the depth of focus. Hence, in an OCT system with fixed sample arm/imaging specimen arrangement, a compromise between lateral resolution and depth scanning range has to be found. Most systems employ a collimated or weakly focused sample beam whose depth of focus is comparable to the A-scan depth. This arrangement yields uniform, but sub-optimal, lateral resolution throughout the entire imaging depth. The use of dynamic focusing enables improved lateral resolution throughout the imaging depth [4–6]. To date, all published designs that incorporate focus compensation are based on bulk/free space optics, which only operate at low scan rates. In addition, the large sizes of these systems preclude their applications in some clinical scenarios, for example endoscopy. Another approach is the use of an axicon lens to maintain a high lateral resolution over a larger depth of field [7]. This design has yet to be tested in biological samples.

Recently, microelectromechanical (MEMS) mirrors have received considerable attention for their potential applications in optical switches, scanners, aberration correction systems, and other optical systems [8,9]. MEMS technologies have also been applied in biomedical research [10]. In OCT imaging, MEMS have been used for transverse beam scanning [11,12]. In this paper, we present a MEMS-based depth focus control system, which is used to axially shift the focus plane of the probe beam synchronously with the depth scanning of the coherence gate. The intention of this study is to develop a high-speed, compact focus control system, which can be integrated into our real-time endoscopic OCT [13,14].

The MEMS mirrors used in this study are 1.4 mm $\times$ 1 mm elliptical deformable mirrors designed for 45° beam incidence angle (Fig. 1). Mirror design and release was carried out at Montana State University (MSU). Mirror fabrication was accomplished by MSU personnel working at Stanford's nanofabrication facility under the auspices of NSF's National Nanofabrication Users Network (NNUN) program. These mirrors have a 3-dB bandwidth in excess of 40 kHz allowing for real-time focus control in imaging systems. The mirror is designed to be used for focus adjustment, with the primary focusing power for the system provided by a fixed objective lens. The mirrors are capable of focal lengths ranging from ∞ to 18 mm. For use in the OCT probe, the mirrors were operated at 8 kHz, synchronously tracking the depth scans of the OCT system.

For a finite conjugate optical system, as is the case for the OCT probe, a hyperbolic reflector allows aberration-free focusing of the incident light. The MEMS mirror emulates a 45° off-axis hyper-

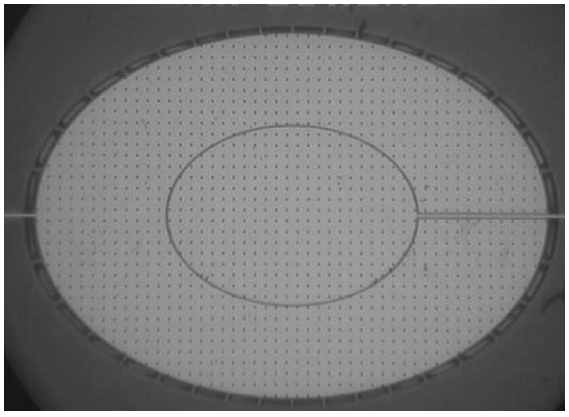

Fig. 1. Twenty times reflectance optical microscope photograph of the MEMS mirror.

boloid reflector, allowing the mirror to be placed in the post-objective optical path of the OCT probe head. The 1.4 mm × 1 mm size results in a 1-mm diameter clear aperture of the optical beam [15].

Fabrication of the deformable mirrors was carried out using a silicon nitride surface micromachining process, the details of which are discussed elsewhere [9,15]. The MEMS mirror was a gold-coated silicon nitride membrane supported by nitride strips along the perimeter. Mirror focusing was achieved using electrostatic actuation, the gold reflective surface serving as the actuating electrode and the underlying silicon substrate as the counter electrode. The actuating electrode consists of two concentric actuation zones. This electrode geometry was used to shape the electrostatic pressure on the membrane in order to control spherical aberration of the mirror. In this proof-of-principle experiment, the two electrodes were kept at the same voltage throughout the scan. The resulting membrane shape approximated the desired hyperbolic surface over the range of displacement necessary to track the OCT gate.

Actuation of the MEMS mirrors was accomplished by applying a bipolar sinusoidal voltage at half the desired scan frequency. The mirror oscillation frequency is twice that of the drive voltage frequency because the electrostatic force is proportional to the square of the voltage [15].

Fig. 2 shows the schematic diagram of the high-speed OCT system used in this experiment. The details have been described in previous publications [13,14]. A 1300-nm broadband light source (JDS, Canada) with a 63-nm bandwidth was used. The coherence length of the source was measured as ~13 μm in air. A Fourier-domain rapid scanning optical delay (RSOD) line was used in the reference arm. Axial scanning was accomplished with an 8-kHz resonant scanner in the RSOD. The 8-kHz sinusoidal monitor signal from the resonant scanner was used as the trigger signal for an arbitrary waveform generator (AWG520, Tektronix, Beaverton, OR), which in turn outputted a 4-kHz signal to a high voltage amplifier (601C, Trek, Medina, NY) connected to the MEMS mirror. The synchrony between the focus scan and the reference arm scan was achieved by using the reference

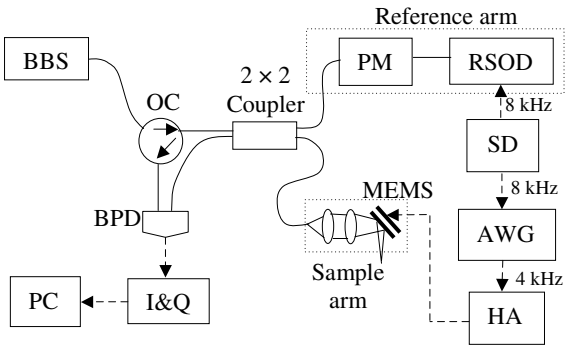

Fig. 2. Schematic of the OCT system. BBS, broadband light source; OC, optical circulator; PM, phase modulator; RSOD, rapid scanning optical delay line; BPD, balanced photo-detector; I&Q, in phase and quadrature demodulator; MEMS, focus control MEMS mirror; SD, scanner driver; AWG, arbitrary waveform generator and HA, high voltage amplifier.

arm's 8 kHz monitor signal to trigger the focus tracking system.

The details of the OCT sample probe optics are shown in Fig. 3. The NA of the probe beam (without MEMS deflection) was about 0.06.

To ensure the focus plane of probe beam always coincided with the coherence gate during an axial scan, the amplitude, phase, and shape of the output signal from the AWG were optimized. The optimal waveform of the driving signal depended on the response of the individual mirror. In our preliminary study, an approximate waveform was deduced as follows.

Driven by a sinusoidal signal, the displacement of the coherence gate relative to its position with the RSOD mirror at 0° can be expressed as:

$$\Delta Z(t) = A\sin(\omega t). \tag{1}$$

Suppose the driving signal on the MEMS mirror is

$$V = V_0 \sin(\omega t/2 + \phi_0). \tag{2}$$

Then the displacement δ at the center of the mirror can be described as

$$\delta(t) = kV^2 = kV_0^2 \sin^2(\omega t/2 + \phi_0), \tag{3}$$

where k is a constant on the order of 10^{-4}–10^{-5} μm/V^2. The focal length of the MEMS mirror f_m can be calculated from

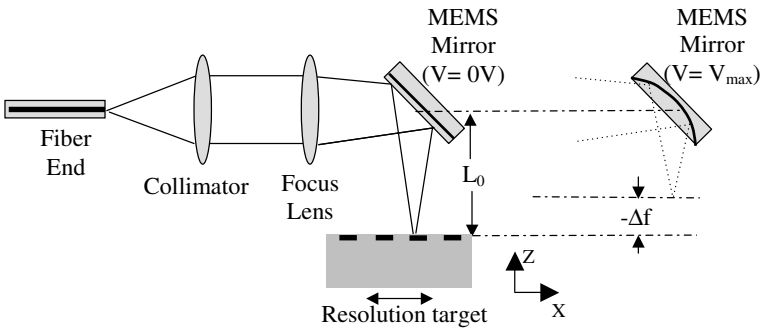

Fig. 3. Schematic of the probe optics.

$$f_{\mathrm{m}}(t) = \frac{D^2}{16\delta} = \frac{D^2}{16kV_0^2 \sin^2(\omega t/2 + \phi_0)} = \frac{f_{\min}}{\sin^2(\omega t/2 + \phi_0)}, \quad (4)$$

where D is the full width of the mirror along its minor axis, δ is the maximum mirror deflection and $f_{\min}$ is the minimum focal length of the MEMS mirror. With the setup shown in Fig. 3, the MEMS-induced shift of the focal point from its initial position (at $V = 0$ V) was

$$\Delta f(t) = \frac{-L_0^2}{f_{\mathrm{m}}(t) + L_0}, \quad (5)$$

where L_0 was the distance from the MEMS mirror to the initial focus point. The minus sign indicates that when a non-zero voltage was applied to the mirror, the focal point of the probe beam moved closer to the mirror.

If $L_0 \ll f_{\mathrm{m}}$ (in our system, L_0 was ~9 mm while f_{m} changed from ∞ at $V = 0$ V to $f_{\min} \approx 60$ mm at $V = 200$ V), then from Eqs. (4) and (5),

$$\Delta f(t) \approx \frac{-L_0^2}{f_{\mathrm{m}}(t)} = \frac{8kL_0^2V_0^2}{D^2}\left(\sin\left(\omega t + 2\phi_0 + \frac{\pi}{2}\right) - 1\right) = \frac{-L_0^2}{2f_{\min}(t)}\left(\sin\left(\omega t + 2\phi_0 + \frac{\pi}{2}\right) - 1\right). \quad (6)$$

Comparing Eq. (1) and Eq. (6), the scan of the focus point was seen to have the same frequency and waveform as that of the coherence gate. If the condition $L_0 \ll f_{\mathrm{m}}$ does not hold then a non-sinusoidal focus control waveform is required. The synchrony between the focus scan and coherence gate scan was achieved in our experiment by adjusting the phase shift ϕ_0 and amplitude V_0 until maximum signals from a sample mirror located at different axial positions were seen.

The voltage-focal length behavior of the MEMS mirror was determined by measuring the static focal length of the probe beam. A mirror was imaged using the optical probe and the mirror position was then adjusted to maximize the reflected signal. By varying the voltage and adjusting the sample the focal length-voltage graph shown in Fig. 4 was made. Fig. 4 shows the measured data

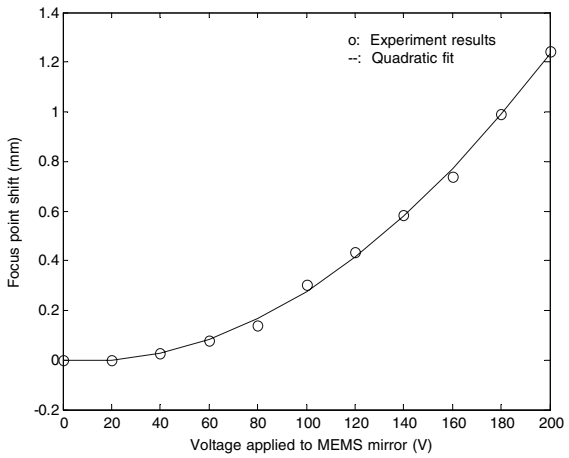

Fig. 4. The response of the MEMS mirror. The X-axis represents the amplitude of the DC signal that was applied to the MEMS mirror. The Y-axis represents the shifts of the focus point.

in agreement with the quadratic dependence of focal shift on applied voltage described in Eq. (6).

Based on these results, a $V_{p-p} = 400$ V sinusoidal signal (±200 V) was delivered to the MEMS mirror, producing a 1.25-mm focus scan range. During the experiment, the depth range of the OCT coherence gate was adjusted to match the range of the focus scan.

To confirm the feasibility of the focus control system, a United States Air Force (USAF) resolution target was imaged by the OCT system with and without a driving signal on the MEMS mirror. The schematic in Fig. 5(a) suggests that without dynamic focus control, the lateral resolution would drop quickly as the target moves out the focus zone. In contrast, with MEMS dynamic focus tracking, the lateral resolution should remain constant across all axial target locations, as depicted in Fig. 5(b).

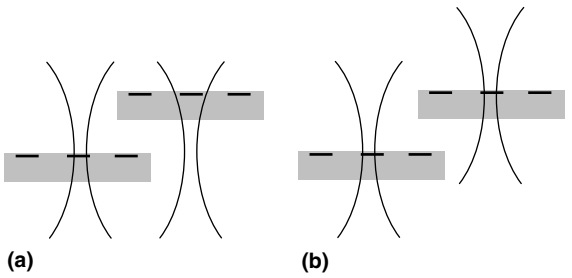

Fig. 5. A schematic comparing imaging conditions with fixed focus and with dynamic MEMS-controlled focus. (a) Without dynamic focus tracking, the lateral resolution is degraded when the specimen is outside of the depth of focus. (b) With dynamic focus control, the focal point is shifted with depth scanning, so that the imaged specimen is always in the probe beam's focal point.

The corresponding experimental results are shown in Fig. 6. First, without a driving voltage, the MEMS mirror functioned as a simple reflector. The USAF target was placed at different distances from the focal plane and images of the 50 μm bars were acquired by the OCT system. A translation stage was used to laterally scan the target. The depth scan range was ~1.25 mm while the lateral scan range was ~0.5 mm. Limited by the speed of the translation stage, each lateral scan took about 2 s. The results are shown in Fig. 6(a). (To see the target clearly, only a limited depth range of the image is displayed.) As the target moved away from the focal plane ($Z = 0$ mm) by more than 0.7 mm, the 50-μm bars become increasingly blurred.

In Fig. 6(b), similar images are shown with MEMS focus scanning active. Even when the target was translated vertically by more than 1 mm from its original position, the 50-μm bars are still clearly resolved when MEMS-activated dynamic focus control was enabled.

These results demonstrate the feasibility of a high-speed focus control system based on a MEMS mirror. Appreciation of the improvement in lateral resolution in 2D biological OCT images requires implementation in a system with higher numerical aperture. Increasing the NA will decrease the focus adjustment range Δf, since the

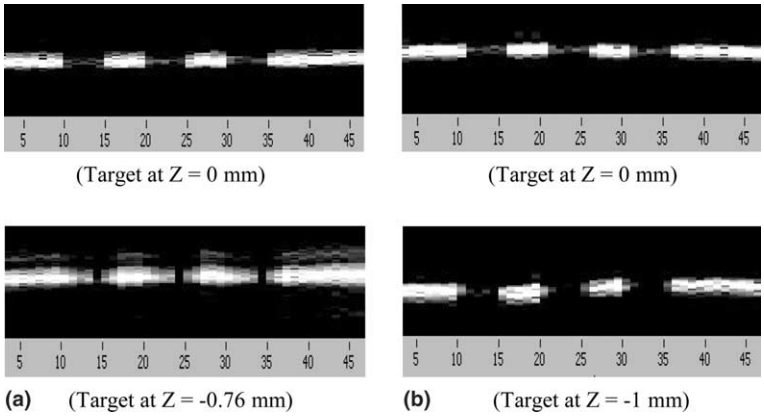

Fig. 6. Images of the 50-μm bars on a USAF resolution target. (The lateral step size was 10 μm.)

focus scan range and the NA of the probe beam are coupled. Redesign of the probe optics to increase one will unavoidably reduce the other. In fact, the product $|\Delta f| \cdot \mathrm{NA}^2$ is a constant during the optical transform of lens system. It can be shown that:

$$|\Delta f| = \frac{nD^2}{4\mathrm{NA}^2 f_{\min}(1 + L_0/f_{\min})}, \tag{7}$$

where D is the diameter of MEMS mirror, n is the refractive index of the sample, and $f_{\min}$ is the minimum focus length of the MEMS mirror at its maximum deflection/highest driving voltage. Eq. (7) may be recast in terms of the depth-of-focus of the imaging beam. Assuming a Gaussian beam with the $1/e^2$ intensity radius coincident with the mirror radius, one depth of focus in the sample is $2nz_0$ with z_0 equal to the Rayleigh range of the beam in air. Then the focus adjustment range may be written as

$$|\Delta f| = \frac{2\pi\delta_{\max}}{\lambda} \frac{1}{(1 + L_0/f_{\min})}(2nz_0), \tag{8}$$

where $\delta_{\max}$ is the maximum displacement of the mirror center. A mirror with larger displacement $\delta_{\max}$ is desired to adjust the focus over many depths-of-focus, permitting the use of a large NA as needed for high-resolution subsurface imaging. In our experiments, the displacement of the MEMS mirror was approximately 1 μm, in order to match the focus scan range to the delay range. This displacement value corresponded to scanning 4.6 times the depth-of-focus of our system. Displacements as great as 5 μm for similar mirrors have been measured, corresponding to 23 depths-of-focus and the potential for use in a correspondingly higher NA system.

In this paper, we presented a focus control system based on MEMS technology. The MEMS mirror device was used in a high-speed OCT system and we demonstrated its feasibility of operation synchronous with the 8 kHz OCT depth scan frequency. Preliminary experimental results with a USAF target showed substantial improvement in the image quality at different target depths. Governing equations relating mirror properties to sample beam focus tracking have been derived. This approach will allow subsurface OCT tissue imaging with improved lateral resolution throughout the imaging depth. Based on these considerations, we anticipate a high NA and large deformation MEMS mirror system compatible with endoscopic imaging.

Acknowledgements

This work was supported by the Natural Science and Engineering Research Council of Canada, the Canadian Institutes for Health Research, Canada Foundation for Innovation, Photonics Research Ontario and the United States National Aeronautics and Space Administration.

References

[1] D. Huang, E.A. Swanson, C.P. Lin, J.S. Schuman, W.G. Stinson, W. Chang, M.R. Hee, T. Flotte, K. Gregory, C.A. Puliafito, J.G. Fujimoto, Science 254 (1991) 1178.
[2] J.G. Fujimoto, Nat. Biotechnol. 21 (11) (2003) 1361.
[3] W. Drexler, U. Morgner, F.X. Kärtner, C. Pitris, S.A. Boppart, X.D. Li, E.P. Ippen, J.G. Fujimoto, Opt. Lett. 24 (17) (1999) 1221.
[4] J.M. Schmitt, S.L. Lee, K.M. Yung, Opt. Commun. 142 (1997) 203.
[5] Z. Chen, T.E. Milner, D. Dave, J.S. Nelson, Opt. Lett. 22 (1997) 64.
[6] F. Lexer, C.K. Hitzenberger, W. Drexler, S. Molebny, H. Sattmann, M. Sticker, A.F. Fercher, J. Mod. Opt. 46 (3) (1999) 541.
[7] Z. Ding, H. Ren, Y. Zhao, J. Stuart Nelson, Z. Chen, Opt. Lett. 27 (4) (2002) 243.
[8] H. Ukita, Opt. Rev. 4 (6) (1997) 623.
[9] P.A. Himmer, D.L. Dickensheets, R.A. Friholm, Opt. Lett. 26 (16) (2001) 1280.
[10] D.L. Polla, A.G. Erdman, W.P. Robbins, D.T. Markus, J. Diaz-Diaz, R. Rizq, Y. Nam, H.T. Brickner, A. Wang, P. Krulevitch, Annu. Rev. Biomed. Eng. 2 (2000) 551.
[11] J.M. Zara, S. Yazdanfar, K.D. Rao, J.A. Izatt, S.W. Smith, Opt. Lett. 28 (8) (2003) 628.
[12] Y. Pan, H. Xie, G.K. Fedder, Opt. Lett. 26 (24) (2001) 1966.
[13] V.X.D. Yang, M.L. Gordon, B. Qi, J. Pekar, S. Lo, E. Seng-Yue, A. Mok, B.C. Wilson, I.A. Vitkin, Opt. Express 11 (7) (2003) 794.
[14] V.X.D. Yang, M.L. Gordon, S.J. Tang, N.E. Marcon, G. Gardiner, B. Qi, S. Bisland, E. Seng-Yue, S. Lo, J. Pekar, B.C. Wilson, I.A. Vitkin, Opt. Express 11 (19) (2003) 2416.
[15] P.A. Himmer, D.L. Dickensheets, Proc. SPIE 4895 (2003) 296.